nature communications

Article

https://doi.org/10.1038/s41467-026-70672-0

Saccades orchestrate intraocular glucose dynamics to shape visual responses in birds

Received: 24 April 2025

Accepted: 27 February 2026

Published online: 13 March 2026

Check for updates

Xi Xu[1,2,5], Tong Xiao[1,2,5], Yibing Chen[1,3,5], Lijuan Song[1,2], Chen Wu[1], Qian Wang[1], Tao Zhang[2,4] & Yan Yang[1,2]

Birds exhibit remarkable vision despite lacking the classical retinal vasculature, raising an enigmatic question about how avascular retinas fulfill energy demands necessary for sight. Avian saccades couple rapid gaze shifts with cyclotorsional oscillations. In pigeons, we show that these saccades orchestrate intraocular metabolic dynamics and visual processing. Using combined measurements of eye movements, intraocular glucose, and neuronal activity in retinorecipient brain regions, we found that saccades induce intraocular glucose fluctuations that are closely linked to changes in visual responses over seconds to minutes. Pharmacologically manipulating glucose availability or eliminating saccadic oscillations produced corresponding changes in neuronal responses, demonstrating causality. Thus, stimulus-driven saccades not only serve visual exploration but also propel retinal metabolism, facilitating neuronal visual responses in the absence of retinal vasculature. These findings underscore an intrinsic interplay among eye movements, metabolic regulation, and visual function, offering insight into how oculomotor behavior supports retinal health and visual performance across species.

Birds present a fascinating paradox in vertebrate evolution: despite exhibiting exceptionally high retinal metabolism among their brain regions[1,2], and possessing larger eyes[3,4], superior visual acuity[5–8], and thicker retinas than mammals[9–11], they entirely lack retinal blood vessels[12–14] that are essential for nutrient delivery in primates[15–17]. This raises an intriguing enigma: how do avian eyes fulfill the intense metabolic activity of thick, high-acuity retinas in the absence of direct vascular support? Solving this puzzle requires uncovering the sophisticated strategies that birds have developed to sustain retinal health and visual performance without conventional vascularization. One potential mechanism centers on avian saccades, rapid, repetitive eye movements that combine a displacement of eye position and several cycles of cyclotorsional oscillation (Fig. 1a; Supplementary Fig. 1a)[18,19]. Composing approximately 10–25% of total viewing time, these saccades have been recognized for orienting gaze and exploring the visual environment[20–28]. Emerging evidence, however, suggests that avian saccades may also facilitate intraocular nutrient transport[29], by acting as mechanical "agitators". Through repetitive motion, these saccades could propel glucose and other nutrients from the pecten oculi toward the retina, ensuring metabolic support to retinal neurons[4,30]. The pecten oculi is a comb-like, pigmented vascular structure unique to birds (Supplementary Fig. 1b) and is considered homologous to the reptilian conus papillaris[31,32], possibly representing an ancient archosaur feature secondarily lost in mammals.

These striking properties of avian eyes led us to hypothesize that their interplay may create a dynamic system for visual processing, driven by three interconnected mechanisms. First, saccades are initiated for exploring visual information and sustaining retinal nutrient levels. Second, these eye movements facilitate the transport of metabolic substances, such as glucose[33], from the pecten oculi into the retina. Third, the resulting nutrient fluxes, especially the fluctuations in glucose levels, may dynamically modulate retinal function[34]. Despite

[1]State Key Laboratory of Cognitive Science and Mental Health, Institute of Biophysics, Chinese Academy of Sciences, Beijing, China. [2]University of Chinese Academy of Sciences, Beijing, China. [3]Sino-Danish Center for Education and Research, University of Chinese Academy of Sciences, Beijing, China. [4]State Key Laboratory of Cognitive Science and Mental Health, Institute of Psychology, Chinese Academy of Sciences, Beijing, China. [5]These authors contributed equally: Xi Xu, Tong Xiao, Yibing Chen. e-mail: yyang@ibp.ac.cn

https://doi.org/10.1038/s41467-026-70672-0

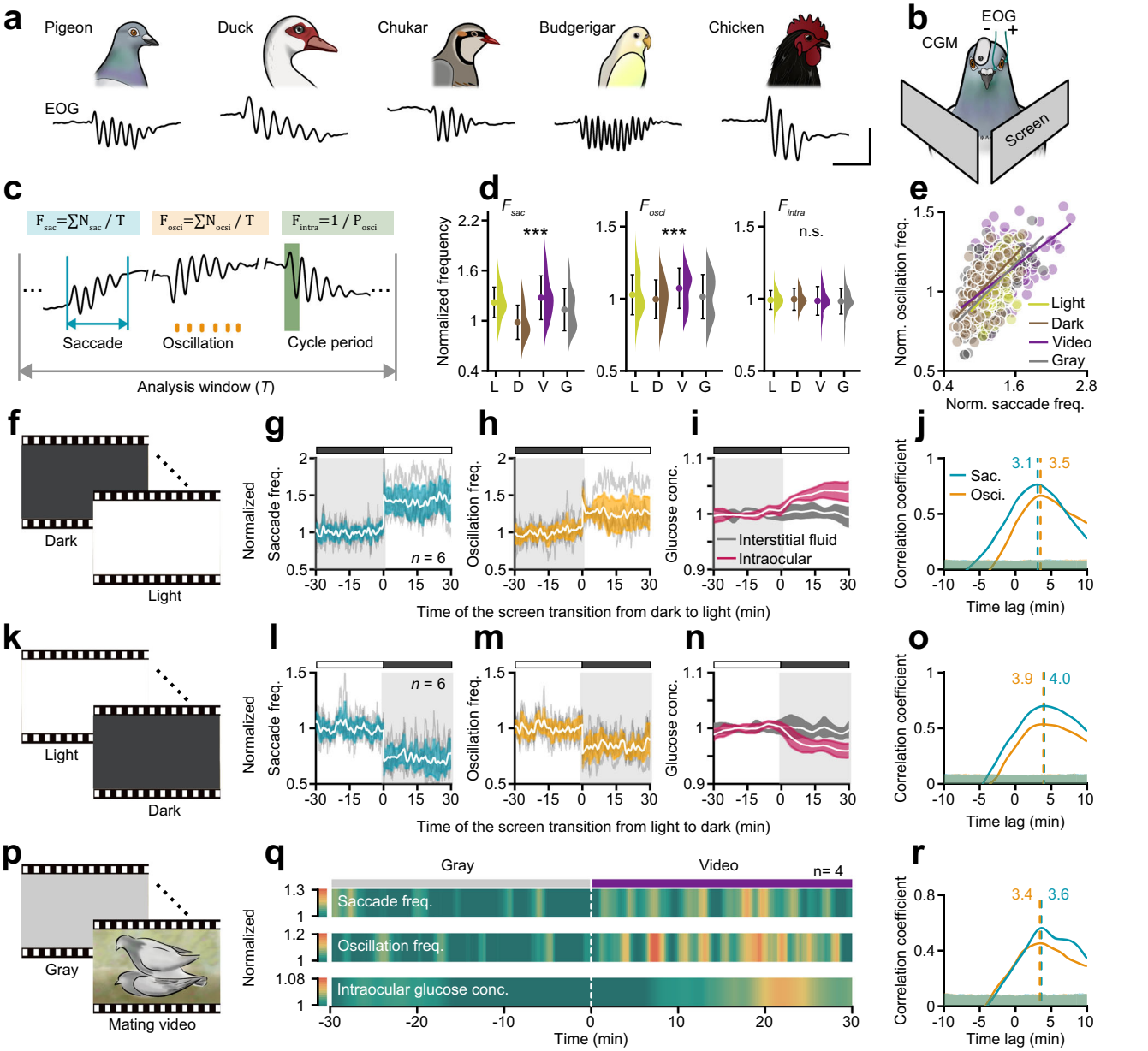

Fig. 1 | Avian saccades driven by visual stimuli are correlated with intraocular glucose levels. a Example electrooculography recordings of saccades from five avian species: pigeon, duck, chukar, budgerigar, and chicken. Scale bars (left to right): 150 ms; 0.28, 0.25, 0.20, 0.34, and 0.25 mV. **b** Schematic drawing of the intraocular glucose monitoring (CGM) and eye movement (EOG) recording systems in awake, head-fixed pigeons[35–37] viewing bilateral visual displays. **c** The definition of saccade frequency, oscillation frequency, and intrasaccadic frequency. **d** Comparison of three frequencies under different visual conditions: light (L), dark (D), gray (G) screens and social mating videos (V) (one-way ANOVA: saccade frequency: $n = 87$ (L), 115 (D), 287 (G), 286 (V), $F_{(3,771)} = 45.26$, $p < 0.001$, oscillation frequency: $n = 86$ (L), 115 (D), 288 (G), 283 (V), $F_{(3,768)} = 11.32$, $p < 0.001$, intrasaccadic frequency: $n = 82$ (L), 111 (D), 290 (G), 286 (V), $F_{(3,765)} = 0.79$, $p = 0.50$). Violin plots depict the distribution of measurement frequencies, whereas bar plots show the normalized mean frequencies for each visual condition, averaged across three pigeons (mean ± SD). *** $p < 0.001$, n.s. not significant. **e** Relationship between saccade frequency and oscillation frequency under four conditions. **f** Schematic diagram illustrating the dark-to-light screen transition. Normalized traces of saccade frequency (**g**), oscillation frequency (**h**), and glucose levels (**i**) during the transition from dark to light screens. The white lines with color shading represent the mean ± SD ($n = 6$ pigeons), and the gray lines indicate data from individual animals. **j** Cross-correlation analysis of the time lag between eye movements and intraocular glucose levels aligned to the dark-to-light transition. Dashed lines indicate the peak time lags. The shaded area represents the 95% confidence interval of the null distribution (generated via shuffling), with correlations above this area considered statistically significant. **k**–**o** Same as (**f**–**j**), but for the transition from light to dark screens. **p** Schematic diagram illustrating pigeon social mating videos. **q** Average result of four pigeons exhibited increased saccadic eye movements and intraocular glucose levels while viewing 30-min conspecific social mating videos. **r** Same cross-correlation analysis as in (**j**), but aligned to the switch to social video. The shaded area represents the 95% confidence interval of the null distribution (generated via shuffling). Source data are provided as a Source data file.

the compelling nature of these hypotheses, they have rarely been investigated as a cohesive entity, leaving critical gaps in our understanding of how avian eyes function without direct vascularization. Previous work has approached the avian saccade as an isolated, static event by measuring the leakage of dye from the pecten following a single saccade[29]. The challenge remains to establish cause-and-effect relationships among saccades, dynamics of intraocular metabolism, and changes in neuronal responses during viewing of visual stimuli.

Here, we address this challenge using an integrated series of experiments designed to test whether and how saccades drive fluctuations in intraocular glucose, and in turn, modulate visual responses in awake, head-fixed pigeons[35–37]. We monitored eye movements and intraocular glucose levels while recording from neurons in three critical retinorecipient nuclei, key structures receiving direct input from retinal ganglion cells and essential for avian visual processing[22,38–45]. We found that saccades induce fluctuations in intraocular glucose and dynamically correlate with changes in neuronal responses over timescales. Furthermore, pharmacological manipulation of both intraocular glucose and saccades resulted in corresponding shifts in neuronal visual responses, establishing causal links. These findings provide direct causal evidence showing how saccades and glucose dynamics interact to shape visual processing in birds.

Results

Saccades elicited by visual inputs are linked to intraocular glucose perfusion

Birds, like primates, make saccades to explore and sample their visual environment[23–28]. However, unlike primates, avian saccades are consistently accompanied by a burst of oscillations spanning tens to hundreds of milliseconds per event, with each oscillatory cycle lasting roughly 20–70 ms depending on species and individual variability (Fig. 1a and Supplementary Fig. 1c–h and Supplementary Videos 1–6). To examine how visual inputs influence avian saccades, we introduced four types of visual stimuli: light, dark, social mating videos, and gray screens, and monitored eye movements (via electrooculography, EOG) in awake, head-fixed pigeons (Fig. 1b)[35–37]. We quantified three frequency-related metrics: saccade frequency (saccade count per 1-min window), oscillation frequency (the total number of oscillatory cycles across all saccades within the 1-min window), and intrasaccadic frequency (the reciprocal of an oscillatory cycle duration) (Fig. 1c). Across distinct visual conditions, both saccade and oscillation frequencies were significantly modulated (Fig. 1d, saccade: $F_{(3,771)} = 45.26$, $p < 0.001$; oscillation: $F_{(3,768)} = 11.32$, $p < 0.001$; one-way ANOVA), whereas intrasaccadic frequency remained unchanged ($F_{(3,765)} = 0.79$, $p = 0.50$). Post-hoc pairwise comparisons identified specific differences between visual conditions, and these findings were further validated using a linear mixed-effects model (LMM) to account for repeated measures from the same animal (Supplementary Fig. 2). Saccade and oscillation frequencies were overall positively correlated across animals and visual conditions (Fig. 1e, dark: $r = 0.63$, $p < 0.001$; light: $r = 0.55$, $p < 0.001$; gray: $r = 0.63$, $p < 0.001$; social video: $r = 0.57$, $p < 0.001$; Pearson correlation), yet their moment-to-moment variations were independent. Residual and cross-correlation analyses revealed no evidence of noise-driven coupling, indicating a shared trend with independent variability in response to visual inputs (all conditions: $r \approx 0$, $p = 1$). Therefore, we focused on saccade and oscillation frequencies in the subsequent analyses.

Previous evidence suggests that such saccadic oscillations may facilitate intraocular glucose perfusion through mechanical agitation of ocular fluids[29]. To investigate how visually-guided saccades influence metabolic regulation, we simultaneously monitored eye movements and intraocular glucose concentrations (via clinical-grade Continuous Glucose Monitoring, CGM) (Fig. 1b). The CGM system provided continuous, real-time glucose assessments (Supplementary Fig. 3a) with accuracy comparable to that of standard glucometers (Supplementary Fig. 3b), and did not significantly alter saccade ($p = 0.63$) or oscillation frequencies ($p \approx 1$, $n = 6$; two-sided Wilcoxon signed-rank test; Supplementary Fig. 3c, d).

By employing 2-h screen-brightness cycles (1 h dark/1 h light; Fig. 1f), we observed that pigeons adjusted their saccadic eye movements in response to luminance changes, accompanied by corresponding dynamic shifts in their intraocular glucose levels. After dark-to-light transitions, saccade frequency increased by 41.66 ± 6.95%, oscillation frequency by 25.62 ± 6.32%, and intraocular glucose levels by 3.35 ± 0.34% ($p_{saccade} < 0.001$, $p_{oscillation} < 0.001$, $p_{glucose} < 0.001$, $n = 6$ pigeons; Fig. 1g–i). Conversely, light-to-dark transitions prompted reductions in saccade frequency (27.26 ± 3.14%), oscillation frequency (16.43 ± 2.60%), and intraocular glucose (2.88 ± 0.58%) ($p_{saccade} < 0.001$, $p_{oscillation} < 0.001$, $p_{glucose} < 0.001$; Fig. 1k–n). Simultaneous interstitial glucose measurements ruled out systemic stress responses (dark-to-light: $p = 0.08$; light-to-dark: $p = 0.41$). A modified lag-correlation analysis revealed that intraocular glucose changes followed fluctuations in saccade and oscillation frequencies by approximately 3–4 min (Pearson correlation; Fig. 1j, o). To further validate this temporal relationship, we applied a standard-deviation (SD)-based threshold method to estimate response latency (see Methods for details). Consistent with the lag-correlation results, this analysis confirmed that glucose responses lagged behind saccade-related changes by roughly 3–4 min across animals (Supplementary Fig. 4).

To determine whether naturalistic visual conditions elicit comparable effects, pigeons were introduced with 30-min conspecific social mating videos preceded by a randomly varying 30–40 min gray screen (Fig. 1p). Pigeons displayed robust increases in both saccadic eye movements and intraocular glucose levels. Across four individuals, saccade frequency, oscillation frequency, and intraocular glucose concentration increased by 7.70 ± 4.97%, 7.97 ± 4.90%, and 2.25 ± 2.80%, respectively, relative to the gray-screen baseline ($p_{saccade} < 0.001$, $p_{oscillation} < 0.001$, $p_{glucose} = 0.03$). The modified correlation analysis revealed a similar temporal lag of approximately 3–4 min between glucose levels and both saccade and oscillation frequencies during the video-viewing condition (Fig. 1r). Together, these findings indicate that visually driven saccades in birds are associated with intraocular glucose mobilization that occurs with a temporal lag of several minutes, providing a delayed boost in nutrient supply during visual information gathering.

Saccades dynamically correlate with retinorecipient neuronal responses across timescales ranging from seconds to minutes

To explore whether saccades modulate neuronal visual responses, we targeted three crucial retinorecipient nuclei that receive direct retinal input and subserve distinct functions within the avian visual pathways. Using a large-field still grating that nearly filled the pigeons' right visual field, we simultaneously monitored eye movements and conducted extracellular recordings in these nuclei. To evoke robust visual responses, the grating periodically moved at 8°/s for 300 ms at random intervals (6–10 s), with motion direction optimized for each neuron's preference (Fig. 2a; Supplementary Fig. 5). This stimulus design minimized interference from eye movements-related artifacts and well controlled retinal slip (Supplementary Fig. 6). In total, we recorded 127 neurons: 57 in the optic tectum (OT) of the tectofugal pathway, 20 in the nucleus opticus principalis thalami (nOPT) of the thalamofugal pathway, and 50 in the pretectal nucleus lentiformis mesencephali (nLM) of the accessory optic system (Fig. 2b). Notably, we analyzed only visual responses that recorded during stable fixation periods between saccades, when perisaccadic influences had fully subsided (see "Methods" for details). This criterion enabled systematic probing of visual responsiveness under steady fixation while eliminating perisaccadic modulations.

We next investigated how variability in visual responses of retinorecipient neurons related to preceding saccadic eye movements across timescales. Eye movements occurring over a series of analysis windows from 1 s to 8 min prior to grating motion onset were analyzed in 1-s increments (example neuron in Fig. 2a). Using a representative 3-min analysis window as an example, both saccade and oscillation frequencies significantly correlated with neuronal visual responses (example neuron: saccade in Fig. 2c: $r = 0.38$, $p < 0.001$; oscillation in Fig. 2d: $r = 0.22$, $p = 0.01$; $n = 120$ trials, Pearson correlation). Because saccade and oscillation frequencies exhibited partially shared

https://doi.org/10.1038/s41467-026-70672-0

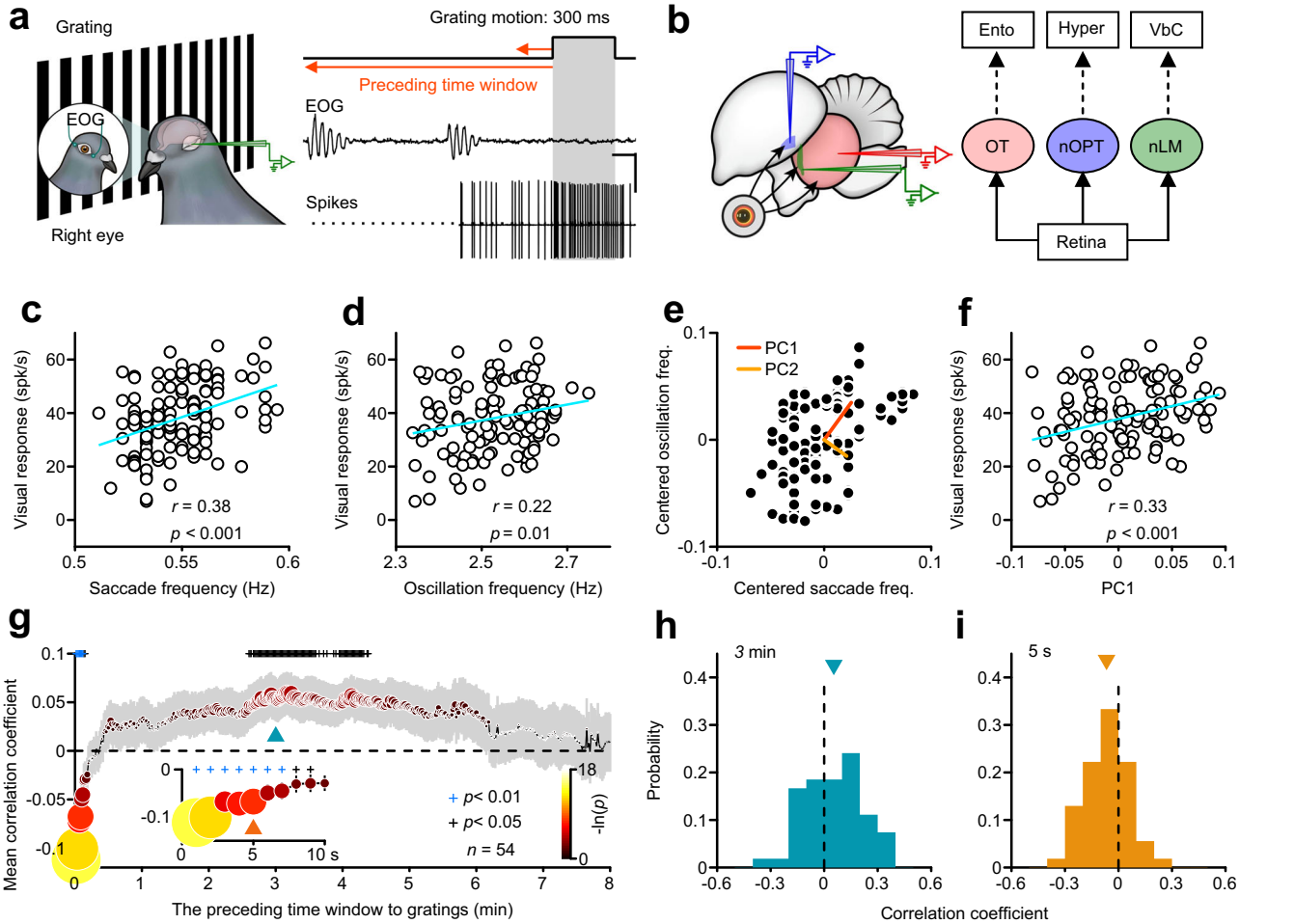

Fig. 2 | Saccades dynamically correlate with visual responses in retinorecipient neurons across both second- and minute-timescales. a Schematic of simultaneous recordings of eye movements and neuronal activity in pigeons during exposure to grating motion. Right: Representative raw traces of EOG and single-neuron activity, with gray shading marking grating motion. The reddish-orange arrow points to the preceding time window analyzed for saccades prior to grating motion. Scale bars: 100 ms; 0.33 mV (EOG); 0.5 mV (spikes). **b** Recordings targeted brain regions receiving direct retinal projections: OT, nOPT, and nLM. The right panel illustrates the three principal avian visual pathways. Ento, Entopallium; Hyper, Hyperpallium; Vbc, Vestibulocerebellum. Example neuron showing the relationship between visual response and saccade frequency (**c**) and oscillation frequency (**d**) within a 3-min analysis window preceding grating motion. Each dot represents one grating-motion trial; lines indicate linear fits. Pearson's *r* and *p* values are shown (two-sided). **e** Principal component analysis of saccade and oscillation frequencies assessed by the 3-min window. **f** Correlation between visual responses of the example neuron and PC1 derived from PCA in (**e**). Data were analyzed using two-sided Pearson correlation. **g** Population analyses showing correlation coefficients between PC1 and neuronal visual responses across preceding time windows of varying durations from 1 s to 8 min. Symbol size and color reflect the degree of statistical significance, represented as $-\ln(p)$ ($n = 54$ neurons, two-sided Wilcoxon signed-rank test; $p < 0.05$ and $p < 0.01$ denoted by plus signs in black and blue, respectively). Gray shading represents 1 SEM. The inset highlights result for time windows ≤10 s. The sky-blue and orange upward triangles indicate the 3-min and 5-s time windows, respectively. Population distribution of correlation coefficients across all 54 neurons for the 3-min (**h**) and 5-s (**i**) time windows. Source data are provided as a Source data file.

variability in response to visual stimuli (Fig. 1e), we utilized principal component analysis (PCA) to quantify their combined effects. PCA decomposed eye-movement metrics into principal components for each neuron (example neuron in Fig. 2e). Correlation analysis demonstrated a significant positive relationship between the first principal component (PC1) and corresponding neuronal visual responses ($r = 0.33$, $p < 0.001$; Fig. 2f). This indicates that higher saccade activity during the preceding period was associated with enhanced neuronal activity.

For population analyses, we focused on 54 out of 127 neurons that had at least 35 repetitions of the moving grating per analysis window, with window lengths extended up to 8 min. Across this population, retinorecipient neurons revealed correlations at both second- and min-scale delays between their visual responses and preceding eye-movement dynamics, including saccade frequency, oscillation frequency (Supplementary Fig. 7), and the combined principal component of both measures (Fig. 2g, h). On a minute-scale, positive correlations emerged approximately 3–4 min before stimulus onset ($n = 54$, $p < 0.05$; Supplementary Fig. 7a, c). Notably, this interval aligns with the delay observed between saccadic eye movements and intraocular glucose changes (Fig. 1). It suggests that saccades may modulate intraocular glucose delivery within this timeframe, thereby influencing retinal sensitivity and subsequent neuronal processing at higher visual regions. Conversely, on a second-scale, negative correlations appeared within the first 10 s, particularly pronounced during the initial 5–7 s ($p < 0.01$; Fig. 2g, i; Supplementary Fig. 7b, d), indicating a transient suppressive effect likely driven by one or two of the most recent saccades. Permutation tests confirmed significant correlations between neuronal responses and saccadic metrics, including their PC1, with both second- and minute-scale delays, indicating that saccade-related measures capture the most robust coupling across timescales (Supplementary Fig. 8).

To quantify these temporal dynamics in more details, we applied sliding-window analyses to compute time-lagged cross–correlations between saccade measures and visual responses (Supplementary Fig. 9). The resulting significance maps revealed that correlations for saccade frequency and the PCA-derived component were most pronounced within bands spanning around 0 s lags with ~150–250 s windows and extending to ~160 s lags with ~10–80 s windows (Supplementary Fig. 9a, e). Oscillation frequency showed weaker but comparable patterns, peaking around 0–20 s lags for 20–150 s windows (Supplementary Fig. 9c). These results indicate that neuronal responses are enhanced following approximately 3-min periods of increased saccadic activity, corroborating the minute-scale coupling effect. While focusing on short time lags (0–7 s; Supplementary Fig. 9b, d, f), a transient negative correlation emerged near 0 s lag, consistent with the second-scale analyses. This effect rapidly diminished beyond ~1 s, reflecting the brief suppressive influence of the immediately preceding saccade.

To further dissect the second-scale effect, we examined how each neuron's responses varied with the time elapsed since the latest saccade. As an example, one neuron's visual responses were sorted by these intervals spanning up to 6 s and binned into three stages with equal ranges (Fig. 3a), revealing a linear increase in visual responses as a function of time since the prior saccade onset ($r = 0.43$, $p < 0.001$; Fig. 3b). Across stages, z-scored visual responses rose significantly (one-way ANOVA, $F_{(2,155)} = 13.13$, $p < 0.001$; Fig. 3c). Population-level analyses across the three visual nuclei consistently showed stronger visual responses in stage 3 than in stage 1 (OT: $p < 0.001$; nOPT: $p = 5.1 \times 10^{-3}$; nLM: $p < 0.001$; Fig. 3d–f), with the majority of neurons exhibiting this pattern (OT: 48/57, 84%; nOPT: 16/20, 80%; nLM: 36/50, 72%). Furthermore, visual responses were positively correlated with the time since the latest saccade (OT: $r = 0.44$, $p < 0.001$; nOPT: $r = 0.47$, $p < 0.001$; nLM: $r = 0.36$, $p < 0.001$; Pearson correlation; Fig. 3g–i). These effects persisted after regrouping intervals to ensure equal trial counts (Supplementary Fig. 10).

These second-scale effects may stem from the time required for glucose and other nutrients to diffuse across the retina after each saccade. If so, neurons whose receptive fields lie closer to the pecten should be modulated sooner, reflecting a gradient of glucose availability (Fig. 3j). To test this, we focused on OT neurons with receptive fields at different retinal locations. In the avian optic tectum or the mammalian superior colliculus, visual neurons receive topographically organized retinal projections[46,47]. Recordings were obtained from an anterior region (A 5.00–6.00 mm; $n = 33$ neurons) with receptive fields near the pecten, and a posterior region (A 1.00–1.25 mm; $n = 24$ neurons) located farther away[40,47,48]. Using a one-dimensional diffusion framework incorporating metabolic consumption and saccade-driven mechanical oscillation (see Methods for details), we estimated that glucose reaches anterior retinal regions more rapidly following saccades, generating distinct temporal profiles of nutrient availability across the retina. The model further predicted phase-dependent fluctuations in glucose concentration, producing asynchronous peaks between proximal and distal retinal zones (Fig. 3k). Indeed, visual responses in both anterior and posterior OT neurons tracked these estimated glucose dynamics (Fig. 3l, m). Compared with posterior OT neurons, anterior OT neurons exhibited significantly stronger visual responses across stages (48.04 ± 4.95 spikes/s vs. 24.24 ± 4.35 spikes/s, mean ± SEM, $p < 0.05$). These findings support a diffusion-based mechanism for the second-scale modulation of visual responses, governed in part by the spatial proximity of receptive fields to the pecten and saccade-induced perfusion dynamics.

Under the second-scale modulation, longer saccades encompassing more oscillatory cycles may induce stronger mechanical agitation, thereby enhancing visual responses. To test this possibility, we incorporated saccade duration and the time elapsed since the latest saccade into partial correlation and linear regression analyses across 54 neurons, controlling one variable while examining the other. Significant positive correlations persisted between visual responses and the time since the latest saccade when controlling for saccade duration or oscillatory cycle count (saccade duration: $r = 0.05$, $p < 0.001$; oscillatory cycle count: $r = 0.05$, $p < 0.001$; multiple linear regression; Supplementary Fig. 11a, b), and between visual responses and saccade duration or oscillatory cycle count when controlling for the time since the latest saccade (saccade duration: $r = 0.37$, $p = 0.04$; oscillatory count: $r = 0.02$, $p = 0.04$; multiple linear regression; Supplementary Fig. 11c, d). These findings indicate that saccade duration, or oscillatory cycle count, and the post-saccadic interval each independently contribute to the short-timescale modulation of visual responsiveness, supporting the interpretation that saccades could transiently enhance ocular glucose transport, thereby boosting retinal metabolic supply and visual signal transmission within seconds after saccades.

Intraocular glucose modulation alters visual responses

To investigate how intraocular glucose regulates neuronal visual responses, we locally manipulated intraocular glucose concentrations while simultaneously recording neuronal activity and monitoring eye movements in pigeons. Initially, intraocular glucose levels were elevated via intravitreal microinjections of D-glucose (1 mol/L, 2 µL; see "Methods"), raising intraocular glucose from 15.36 ± 0.40 to 17.69 ± 0.53 mmol/L (mean ± SEM, $n = 9$, $p = 3.9 \times 10^{-3}$). Due to spatial limitations in our recording setup, we focused on retinorecipient neurons in the nLM and measured visual responses to 300 ms grating-motion stimuli (Fig. 4a). In an example neuron, visual responses increased from 23.70 ± 13.22 to 70.23 ± 17.70 spikes/s within 2 min post-injection (mean ± SD, $p < 0.001$; Fig. 4c, d). Across all nine examined nLM neurons, D-glucose administration significantly increased visual responses ($p = 7.8 \times 10^{-3}$; Fig. 4g). The enhancement emerged within approximately 15 s ($p < 0.05$), suggesting a rapid increase in local glucose availability likely facilitated by several saccades occurring over tens of seconds that boosted visual activity. Control experiments with L-glucose and saline injections revealed no significant changes in visual responses on the example neuron (Fig. 4e, f) or across the population (L-glucose: $p = 0.30$, $n = 9$ neurons, Fig. 4h; saline: $p = 0.58$, $n = 7$ neurons, Fig. 4i). The order of these injections (D-glucose, L-glucose, and saline) was randomized for each examined neuron.

We next explored the effects of decreasing intraocular glucose by inhibiting glucose transporter 1 (GluT-1; Fig. 4b), a primary glucose transporter highly expressed in the avian pecten oculi[49,50]. Intravitreal administration of the GluT-1 inhibitor Bay-876 (100 µmol/L, 1 µL)[51–53] effectively reduced glucose concentrations from 15.82 ± 0.34 to 11.52 ± 1.31 mmol/L (mean ± SEM, $p = 2.0 \times 10^{-3}$, $n = 10$ pigeons). This decrease led to reduced visual responses, as illustrated by an example neuron, whose firing dropped from 85.67 ± 24.88 to 47.10 ± 16.21 spikes/s (mean ± SD, $p < 0.001$, Fig. 4p, q). Population analyses of 10 neurons confirmed that lowering intraocular glucose significantly diminished visual responses ($p = 9.8 \times 10^{-3}$; Fig. 4r).

None of these microinjections affected saccade or oscillation frequencies (Fig. 4j–o, s, t) or neuronal spontaneous firing rates ($p > 0.05$). These findings demonstrate that pharmacological manipulation of intraocular glucose, either elevating or reducing it, robustly influences neuronal visual responses. They underscore the critical role of glucose in retinal function and its potential as a key modulator of sensory processing in visual systems.

Muscimol-induced suppression of saccades unmasks glucose-driven modulation of visual responses

To determine how saccades modify neuronal visual responses through changes in glucose levels, we suppressed these eye movements by injecting the $GABA_A$ receptor agonist muscimol into the raphe complex, key brainstem nuclei for saccadic oscillations in pigeons[20,22]. Concurrently, we monitored intraocular glucose concentrations and

https://doi.org/10.1038/s41467-026-70672-0

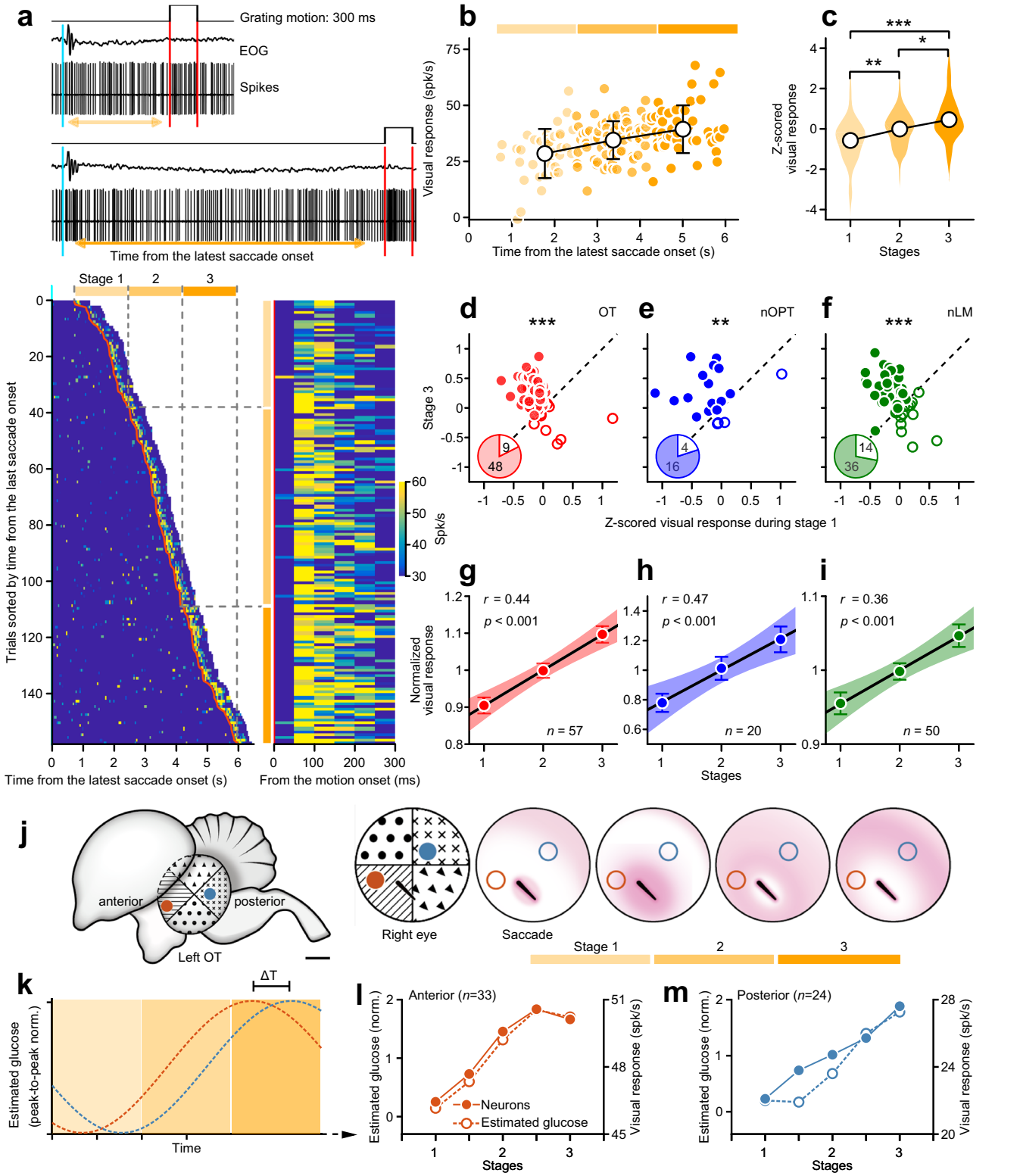

neuronal activity in response to visual stimulation (Fig. 5a). After muscimol injection, both saccade and oscillation frequencies were significantly reduced (saccade frequency: pre-injection, 0.28 ± 0.04 Hz; post-injection, 0.02 ± 0.01 Hz, $p < 0.001$; oscillation frequency: pre-injection, 1.47 ± 0.27 Hz; post-injection, 0.04 ± 0.01 Hz, $p < 0.001$; mean ± SEM, $n = 6$ pigeons; Fig. 5b, c). These reductions were accompanied by a significant decrease in intraocular glucose, from 16.00 ± 2.01 to 11.45 ± 2.08 mmol/L ($p < 0.001$; Fig. 5d). Utilizing the modified lag correlation analysis, we observed that subsequent drops in intraocular glucose lagged behind the reduction in saccade frequency by 3.4 min and oscillation frequency by 3.7 min (Fig. 5e). Independent estimation of glucose latency using an SD-based threshold confirmed a ~3-min delay of glucose changes relative to saccade activity (Supplementary Fig. 4f). These results closely match the temporal lag observed in earlier results (Figs. 1 and 2).

Suppressing saccadic oscillations with muscimol significantly attenuated eye movements and visual responses, as demonstrated by an example neuron (Fig. 5f, g), and confirmed across all three

https://doi.org/10.1038/s41467-026-70672-0

Fig. 3 | Dynamic changes in visual responses following the latest saccade. **a** Example traces of EOG and neuronal spiking activity in response to grating motion. Red lines mark motion onset/offset, while sky-blue lines indicate the latest saccade onset. Visual responses were categorized into three stages based on intervals from the saccade onset, represented by progressively darker yellow shades. Heatmaps depict responses from an example neuron, sorted by time since the latest saccade onset (left) and aligned to grating motion onset (right). Visual responses of the example neuron plotted against time since the prior saccade onset (**b,** $n = 158$ trials) and z-scored distributions across three stages (**c**, one-way ANOVA, $F_{(2,\ 155)} = 13.13$, $p < 0.001$). Post hoc pairwise comparisons were adjusted using the Holm-Bonferroni (adjusted $p_{1,2} = 0.02$, $p_{2,3} = 2.2 \times 10^{-3}$). Comparison of z-scored visual responses between stage 3 and stage 1 for neurons in the OT (**d**), nOPT (**e**, $p = 5.1 \times 10^{-3}$), and nLM (**f**) regions, and their normalized visual responses across three stages (**g**–**i**). Data points represent mean ± SEM. Black lines represent the linear regression, while the shadings are the 95% confidence interval of the fit. **j**–**m** Estimated glucose dynamics following a saccade differ between anterior OT (a-OT, red) and posterior OT (p-OT, blue) neurons due to the proximity of their visual receptive fields to the pecten[40,47,48]. Red and blue dots indicate the recording sites and their respective receptive fields (**j**; Scale bar: 2 mm). Temporal glucose diffusion patterns reveal a delay between a-OT and p-OT neurons (**k**). Estimated glucose dynamics (open circles, dashed lines) showed trends similar to the visual response (filled circles, solid lines) in the a-OT (**l**) and p-OT (**m**) across stages. Data points and error bars represent mean ± SEM. * $p < 0.05$, ** $p < 0.01$, *** $p < 0.001$, two-sided Wilcoxon rank-sum test. Source data are provided as a Source data file.

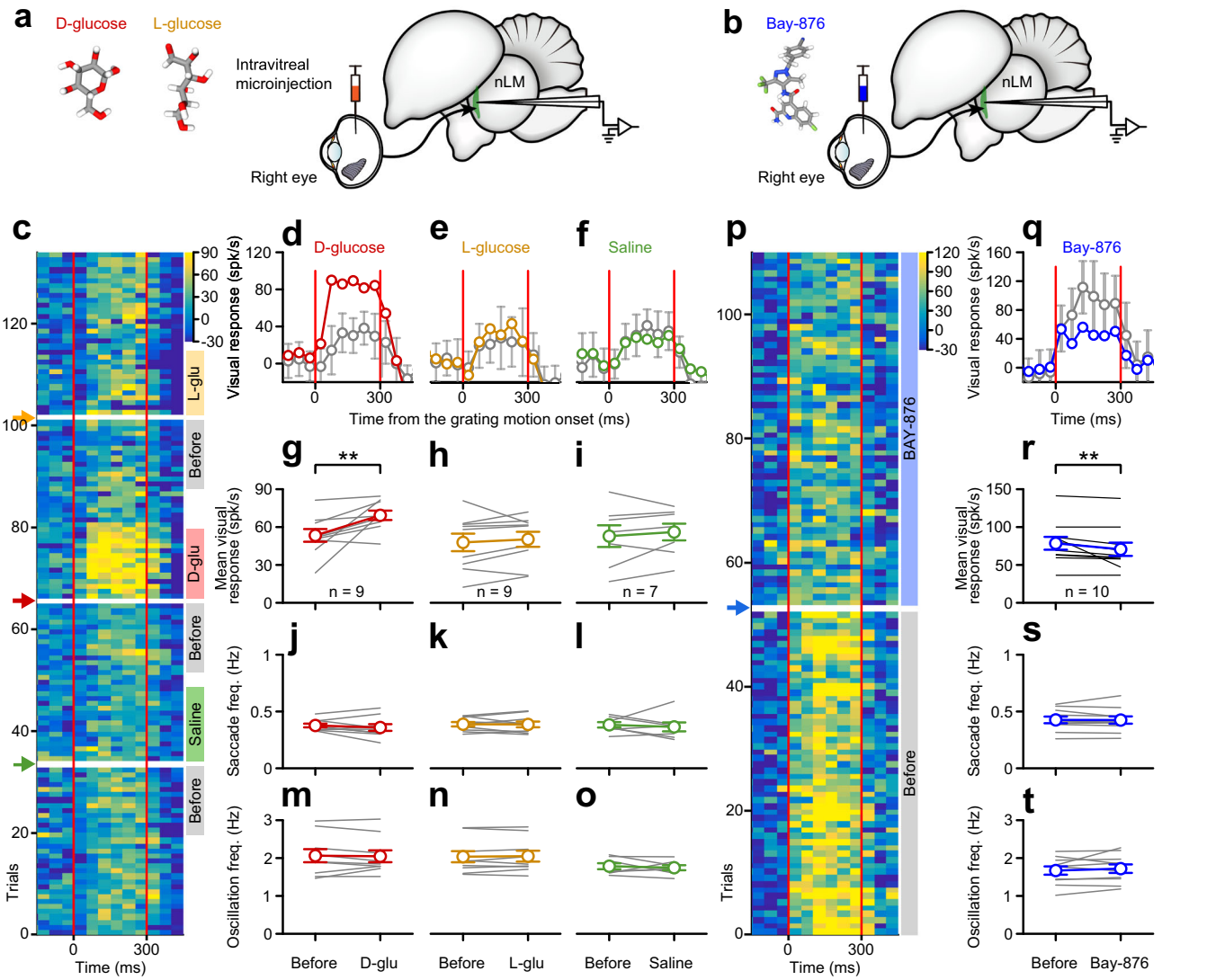

Fig. 4 | Bidirectional intraocular glucose manipulations effectively modulate visual responses. Pharmacological experimental setup illustrating intravitreal microinjections of D-glucose, L-glucose, saline (**a**) or Bay-876 (**b**). **c** Heatmaps showing visual responses of an example neuron to grating motion, before and after intravitreal microinjections of saline, D-glucose, and L-glucose, in order. Colored arrows indicate the time of injections, and colored bands represent analysis windows (2 min). Visual responses before and after intravitreal microinjections of D-glucose (**d**, **g;** $p = 7.8 \times 10^{-3}$ in **g**), L-glucose (**e**, **h**), and saline (**f**, **i**) for the example neuron (**d**–**f**) and the neuron population (**g**–**i**). Saccade frequencies (**j**–**l**) and oscillation frequencies (**m**–**o**) from the same population of neurons (*n* numbers as in **g**–**i**) before and after injections of D-glucose (**j**, **m**), L-glucose (**k**, **n**), and saline (**l**, **o**). **p** Heatmaps of visual responses from an example neuron before and after Bay-876 injection. The blue arrow marks the injection time, and colored bands represent the 10-min analysis windows before and after the injection. Visual responses before and after Bay-876 injection for an example neuron (**q**) and across the neuron population (**r,** $p = 9.8 \times 10^{-3}$). Saccade frequency (**s**) and oscillation frequency (**t**) from the same population of neurons (*n* number as in **r**) before and after Bay-876 injection. **$p < 0.01$, two-sided Wilcoxon signed-rank test. Error bars in (**d**–**f**, **q**) represent mean ± 1 SEM, while (**g**–**o**, **r**–**t**) depict individual neuron data (gray lines) and the mean ± SEM (colored lines). Source data are provided as a Source data file.

https://doi.org/10.1038/s41467-026-70672-0

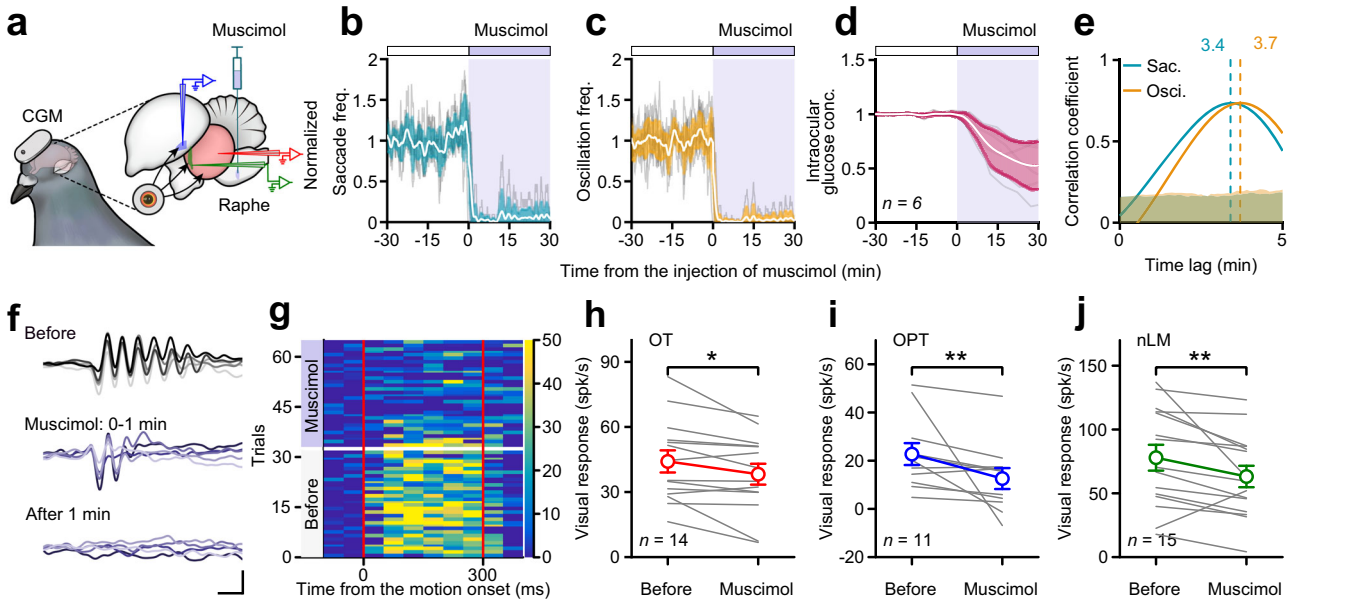

Fig. 5 | A causal link between saccades, intraocular glucose regulation, and visual response modulation. a Schematic of the experimental setup showing muscimol injections into the raphe complex to suppress saccadic oscillation during glucose monitoring and neuronal recordings in OT, nOPT, and nLM. Normalized time-course changes in saccade frequency (**b**), oscillation frequency (**c**), and intraocular glucose levels (**d**) before and after muscimol injections. Thin gray lines represent individual animals, while white lines with colored areas show the population mean ± SD. **e** Cross–correlation analysis of the time lag between saccadic metrics and intraocular glucose levels aligned to muscimol injection. Dashed lines indicate the peak time lags. The shaded area represents the 95% confidence interval of the null distribution (generated via shuffling; see Methods). Saccadic eye movements (**f**) and visual responses of an example neuron (**g**) before and after muscimol injection. Scale bars: 50 ms; 1 mV. Comparison of visual responses to grating motion in the OT (**h**, $p = 0.01$), nOPT (**I**, $p = 6.8 \times 10^{-3}$), and nLM (**j**, $p = 5.4 \times 10^{-3}$) within 10 min before and after muscimol injection. Gray lines represent individual neurons, while colored lines depict the mean ± SEM. * $p < 0.05$, ** $p < 0.01$, two-sided Wilcoxon signed-rank test. Source data are provided as a Source data file.

examined nuclei (Fig. 5h–j). In the OT, neuronal activity to visual stimuli decreased from 44.10 ± 5.10 to 38.22 ± 4.81 spikes/s (mean ± SEM, $p = 0.01$, $n = 14$ neurons; Fig. 5h). Similarly, in the nOPT, visual responses dropped from 22.74 ± 4.54 to 12.59 ± 4.35 spikes/s ($p = 6.8 \times 10^{-3}$, $n = 11$ neurons; Fig. 5i), and in the nLM, declined from 77.89 ± 10.12 to 63.15 ± 8.40 spikes/s ($p = 5.4 \times 10^{-3}$, $n = 15$ neurons; Fig. 5j). In contrast, muscimol had no significant impact on spontaneous neuronal firing ($p_{OT} = 0.67$, $p_{nOPT} = 0.08$, $p_{nLM} = 0.12$). The reduction in visual responses began approximately 4.3 min after muscimol injection across 40 neurons ($p < 0.001$). Considering the 0.5–0.7-min delay between injection and the suppression of saccades (Supplementary Fig. 4f), this corresponds to a comparable 3-min lag between reduced saccade frequency and the onset of neuronal inhibition. Thus, within minutes after saccades cease, both glucose supply and neuronal activity decline almost simultaneously, linking saccade-driven perfusion to visual responsiveness. Together, these findings underscore the critical role of saccades in regulating intraocular glucose and modulating visual responses in retinorecipient neurons. This interplay between eye-movement dynamics and metabolic regulation provides mechanistic insight into how avian retinas sustain high metabolic demands to maintain optimal visual processing.

Discussion

Unlike primates, birds lack retinal blood vessels[12,13] and instead rely on alternative mechanisms to meet the metabolic demands of their thick, high-acuity retinas[2,29,54]. Our findings reveal a dynamic process wherein avian saccades orchestrate intraocular glucose fluctuations that, in turn, shape neuronal visual responsiveness in a temporal manner. Both second- and minute-scale modulations highlight the intricate coupling between eye movements and visual processing. Across distinct visual conditions, we identified a consistent 3–4 min lag between stimuli-driven saccades and subsequent changes in intraocular glucose (Fig. 1), aligning closely with improvements in neuronal responses over the same timeframe (Fig. 2). This minute-scale effect suggests that repetitive saccades progressively enhance retinal responsiveness through saccade-driven glucose delivery. Such a mechanism likely compensates for the absence of retinal vasculature by providing sustained metabolic support for optimal visual performance. More broadly, it reflects a long-timescale metabolic benefit, whereby the cumulative history of saccadic activity supports retinal function in avian species lacking direct vascularization.

In contrast to the minute-scale mechanism, our results also revealed a second-scale modulation, characterized by transient negative correlations between eye movements and neuronal visual responses (Fig. 2g, i). Previous research demonstrated that fluorescein dye disperses about 3 mm from the avian pecten within 2 s after a single saccade, whereas diffusion during fixation was notably limited, less than 0.5 mm even after 120 s, highlighting the inefficiency of passive diffusion mechanisms[29]. Thus, saccades appear to drive nutrient perfusion from the pecten across the avian retina, achieving widespread metabolite distribution within seconds (Fig. 3j). Consistently, our data confirmed that visual responses increased within seconds after individual saccades (Fig. 3), and that neurons with receptive fields nearer to the pecten exhibited earlier and larger enhancements than those farther away (Fig. 3j–m), reflecting a transient spatial gradient in nutrient availability. Both the duration and oscillation count of the last saccade, as well as the interval since it occurred, correlated with visual response strength. Longer saccades likely induced stronger mechanical agitation of intraocular fluid, while longer intervals enabled more time for glucose diffusion to retinal cells. Together, these results suggest a rapid, saccade-driven mechanism that transiently enhances nutrient delivery and visual responsiveness in avian retinas lacking vascular support.

Our pharmacological manipulations provide a causal linkage between saccades, glucose dynamics, and visual neuronal responses. Increasing intraocular glucose with D-glucose (but not the non-

metabolizable L-glucose)[55–57], and decreasing it via the GluT-1 inhibitor Bay-876[51–53], reliably altered neuronal visual responses (Fig. 4). These manipulations confirm that fluctuations in local glucose availability sensitively tuned retinal function, highlighting the critical role of precise metabolic regulation for sustaining high-acuity vision under varying environmental demands. Additionally, inactivation of the brainstem raphe complex via muscimol, a known critical hub for saccade generation in pigeons[20], suppressed saccadic oscillations, subsequently lowering intraocular glucose levels and diminishing visual responses (Fig. 5). These findings identify the pivotal role of saccades in ensuring adequate nutrient supply to retinal neurons.

It should be noted that avian saccades actively contribute to visual processing beyond its classic role in orienting gaze during environmental scanning. Our findings indicate that these saccades may act as visual-stimulus-driven "engines" that regulate intraocular metabolism and visual performance. Salient or arousal visual inputs might elicit more frequent saccadic eye movements, which are accompanied by elevated intraocular glucose levels, effectively propelling metabolic supply to retinal neurons engaged in information processing. This interplay among saccadic eye movements, intraocular metabolic support, and neuronal responses underscores a sophisticated adaptive mechanism tailored to the high-acuity visual demands of birds. Specifically, stimulus-driven enhancement of saccades appears to shape retinal function via glucose availability, enabling birds to cope efficiently with visually demanding environments.

Although our conclusions are grounded in glucose measurements, other metabolic substrates, particularly oxygen, are also likely influenced by avian saccades. Because each substrate could exhibit distinct diffusion and transport kinetics, their relative contributions to retinal metabolism may vary accordingly. While the proposed mechanism that mechanical agitation of eye movements promotes glucose diffusion and availability across multiple timescales provides a plausible explanation for the coexistence of second- and minute-scale effects observed here, direct physiological evidence remains lacking. Future studies combining millisecond-resolution monitoring of multiple metabolic substrates with simultaneous neuronal recordings will be crucial to delineate their precise temporal coupling and validate this mechanistic framework.

Together, these findings uncover a previously unrecognized metabolic dimension of avian saccades, extending their role beyond visual scanning to encompass metabolic and functional optimization. This mechanism may represent an evolutionarily conserved strategy through which eye movements dynamically sustain retinal metabolism and optimize visual performance in birds, potentially extending across species.

Methods

Animal preparation

We performed experiments on forty-seven awake, head-fixed[35–37] adult pigeons (*Columba livia*, body weight 300–500 g; both sexes; wild-type). All animals were purchased from local dealers and housed at the Institute of Biophysics, Chinese Academy of Sciences, under a 12–12 h light-dark cycle. Pigeons were randomly assigned to two sets of behavioral and physiological studies. In the first set, ten pigeons were utilized to investigate saccadic eye movements while viewing social mating videos or alternating light/dark screens; intraocular glucose levels were continuously monitored during these sessions. In the second set, the remaining 37 were evaluated for neuronal visual responses to grating motion stimuli presented in a dimly lit room, associated with pharmacological manipulations. Among them, eighteen animals received muscimol injections targeting the raphe nucleus, nine animals were administrated intraocular injections of D-glucose, L-glucose, and saline in a randomized order, and the remaining ten animals were given an intraocular injection of Bay-876, a potent and selective GluT-1 inhibitor. In the first set of experiments (Fig. 1 and Supplementary Fig. 1), we broadened the evolutionary scope by including four additional adult avian individuals from different species (all wild-type): a budgerigar (*Melopsittacus undulatus*), a chukar partridge (*Alectoris chukar*), a chicken (*Gallus gallus domesticus*), and a muscovy duck (*Cairina moschata*), which diverged tens of millions of years ago[58], to assess their saccadic eye movements. Sex was randomly selected and not included as a biological variable in the study design.

Each animal was anesthetized by injecting ketamine (30 mg/kg) and dexmedetomidine (0.125 mg/kg) into the pectoral muscles. The anesthetic status was monitored by examining their respiration patterns and reflex reactions to toe pinching[20,22,59]. Pigeons were wrapped with soft straps and positioned into a stereotaxic apparatus. After a scalp incision, a lightweight steel head holder was affixed to the skull to ensure stable head restraint in experiments. Guided by stereotaxic coordinates of the pigeon brain[60], recording windows over the left tectum, the left telencephalon, as well as a pharmacological injection window over the cerebellum, were surgically exposed by a dental drill. The overlying dura mater remained intact. We also gently drilled a little fragment of the orbital bone (1 × 1 mm) located on the top of the right eye, for the purpose of intraocular glucose examinations and intraocular injections. After surgery, the scalp was sutured and prescribed erythromycin ointment (BAI-JINGYU Pharmaceutical, Nanjing, China). Pigeons were housed individually and received Meloxicam (0.5 mg/kg, PO, once or twice daily) to alleviate postoperative pain and ceftriaxone sodium (75 mg/kg, IM, every 6–8 h) to prevent infection for 3–7 days. Within 12–24 h, their locomotion, feeding, and hydration behaviors had resumed.

On experimental days, pigeons received a light dose of ketamine (4 mg/kg), were coated in a soft bag, and situated on a foam couch. The head was secured to the stereotaxic apparatus via the implanted head holder. Wound margins and surrounding muscles were periodically infiltrated with lidocaine (Shanghaizhaohui Pharmaceutical, China). Experiments commenced at least 30 min after light ketamine sedation when the animals had recovered, consistent with a prior report[61]. All neuronal recordings were performed in awake, head-fixed pigeons[35–37] with unrestricted eye movements. During neuronal recordings, the left eye was covered while the right eye was exposed to visual stimuli. For monitoring eye movements in the budgerigar, chukar partridge, chicken, and duck, animals underwent the same anesthesia and head-fixation procedures. During the experiments, animals were not provided with food or water; however, they had free access to both in their home cages before and after each session.

All procedures in this study were in strict accordance with the guidelines for the care and use of animals established by the Society for Neuroscience. All of the animals were handled according to protocols approved by the Institutional Animal Administration Committee at the Institute of Biophysics, Chinese Academy of Sciences (IBP-P-001(21) and IBP-P-001(24)).

Visual conditions

The study introduced three types of visual stimuli to the animals, programmed using Psychtoolbox-3 (version 3.0.18) and executed within the MATLAB platform (R2016b, MathWorks Inc., USA). Mating videos and light/dark stimuli were presented on two 27-inch computer screens (Q27P2, AOC, China) positioned around the viewer's head (Fig. 1b). In the video experiments, pigeons were first presented with a gray screen for a randomly varying period of 30–40 min, followed by a 30-min presentation of mating videos (Fig. 1p). For light/dark stimuli, the screens alternated between white (RGB: 255, 255, 255) and black (0, 0, 0) at 60-min intervals (Fig. 1f, k). During white-screen presentations, the luminance at the animal's eye position was measured at 199.3 ± 0.7 lux, while black-screen presentations had a luminance of 3.0 ± 0.0 lux (LX-1330B lux meter, Tondaj, China). Each behavioral session lasted approximately 3–4 h per experimental day.

To investigate neuronal visual responses, the visual stimuli used were full-field square wave gratings with a spatial frequency of 0.16 cycles per degree. The grating was displayed on a large screen (130° × 140°) positioned 50 cm from the viewer's right eye using an EPSON CB-535W projector. The grating field's horizontal and vertical meridians were rotated by 38° to match the pigeon's natural viewing conditions[62,63]. The luminance of black and white stripes of grating was 0.1 and 6.6 cd/m^2, respectively. The orientation of each grating was orthogonal to its direction of motion. Gratings were presented for 300 ms, moving at 8°/s in one of four cardinal directions: temporal-to-nasal (T–N), nasal-to-temporal (N–T), dorsal-to-ventral (D–V), or ventral-to-dorsal (V–D)[20]. For each neuron, the direction of motion was customized to evoke the strongest visual response (Supplementary Fig. 5). Grating motions lasting 300 ms were randomly introduced with inter-trial intervals ranging from 6 to 10 s. These motion stimuli were designed to probe neuronal responses while preventing the induction of saccadic or optokinetic nystagmus eye movements (Supplementary Fig. 6).

Pharmacological injections

To administer muscimol into the raphe complex, a Drummond™ PCR micropipette (1–10 μL, Thermo Fisher Scientific, USA) was used for microinjection via a PE-21 system (Narishige, Japan) and filled with muscimol (2%, PhytoLab, Germany). Accurate targeting of the raphe complex was achieved by initially inserting a glass-insulated tungsten microelectrode into the target area according to stereotaxic coordinates (from the interaural midpoint, P 0.25 mm, L 0.00 mm). The raphe complex was identified by the presence of well-characterized omnipause neurons, which exhibit a high tonic discharge rate that ceases during saccades in any direction[20,22,64]. Next, the injection micropipette was connected to a gas-pressure microinjection system (Parker Picospritzer III, USA) and advanced into the raphe complex along the same trajectory as the microelectrode. Muscimol was administered in volumes of 20–50 nL. Following injections, pigeons exhibited cessation of saccadic oscillations within approximately 1 min following the injection (Fig. 5f), with normal saccadic activity resuming after roughly 1.5 h.

A custom-developed delivery system was used for the intraocular injections. This system included a sterilized 34-gauge needle connected to a microinjection pump (Zibo Guanjie Electronic Technology, China) via a 1-mL syringe. The microinjection pump was controlled automatically using Spike2 software (version 8.24, Cambridge Electronic Design Limited, UK), enabling precise programming of injection timing and speed. The needle was carefully inserted into the eyeball through a surgically drilled window on the orbital bone, ensuring its tip was positioned in the intraocular fluid. During distinct pharmacological experiments, the following substances were injected intraocularly: D-glucose (1 mol/L, 2 μL, Sinopharm Chemical, China), L-glucose (1 mol/L, 2 μL, Sigma-Aldrich, USA), saline (2 μL, CSPC PHARMA, China), and Bay-876 (100 μmol/L, 1 μL, MedChemExpress, USA). The insertion of the microinjection apparatus itself did not significantly alter saccadic eye movements (saccade: $p = 0.84$; oscillation: $p \approx 1$, $n = 6$, two-sided Wilcoxon signed-rank test; Supplementary Fig. 3e, f).

Electrooculogram recording (EOG)

An electrooculogram system was employed to monitor eye movements[20–22,65]. Two EOG electrodes were carefully implanted into the anterior and posterior regions of the orbital arch, while a third electrode was positioned on the occipital bone as a reference. The eye movement signals were band-pass filtered with a range of 0.1–500 Hz (A-M Systems, Microelectrode AC Amplifier Model 1800, USA). Subsequently, the signals were sampled at a rate of 1000 Hz and stored for offline analysis (CED Power1401, Cambridge Electronic Design Limited, UK).

Assessments of glucose levels

In this study, assessments of glucose levels involve measuring the concentration of glucose in intraocular fluid and interstitial fluid of pectoral muscles, via the Continuous Glucose Monitoring (CGM) systems (Freestyle Libre 2 CGM System, Abbott, USA; GS1 CGM System, SIBIONICS, China) and the glucometer (Accu-Chek Active, Roche, Switzerland). The CGM was conducted using commercially available glucose detection probes to monitor glucose concentrations in the eye and body over hours. The probe was inserted into the eyeball through the surgical window in the orbital bone, landing in the intraocular fluid. The transmitter was secured to the skull using a UV-curing adhesive (ergo 8500 Metal, Kisling AG, Switzerland). A small amount of medical petroleum jelly (Lircon, China) was used to seal the exposed area. A second glucose monitoring probe was inserted into the pectoral muscle and fastened by adhesive tape. These probes are equipped with flexible micro-detection heads that prevent damage to animals' tissue and have a minimal impact on their eye mobility.

We assessed the temporal sensitivity and accuracy of CGM systems to detect changes in glucose concentration. To evaluate temporal sensitivity, a higher concentration glucose solution (1 mL, 15 mmol/L) was introduced into the testing glucose environment (20 ml, 5 mmol/L) 20 s prior to sampling. Subsequent samples were analyzed to determine the system's capability to detect glucose fluctuations. The response was quantified using normalized readings, calculated as CGM change divided by actual concentration change (Supplementary Fig. 3a). For accuracy evaluation, CGM measurements were validated against reference values obtained from a glucometer across glucose concentrations ranging from 2.5 to 20 mmol/L, in increments of 2.5 mmol/L (Supplementary Fig. 3b).

Extracellular recordings

The single-cell recordings utilized custom-made glass-insulated tungsten microelectrodes, which had impedances ranging from 1 to 3 MΩ. The microelectrodes were laterally inserted into the left tectum to specifically target the OT (A 5.00–6.00 mm) and the nLM (A 5.50–6.00 mm, L 4.00 mm; H 5.50–6.00 mm), and vertically introduced through the left telencephalon to target the nOPT (A 6.5–7.0 mm, L 2.8–3.2 mm, H 7.0 mm). The neuronal signals underwent filtration using a band-pass filter with a range of 300–5000 Hz (A-M Systems, Microelectrode AC Amplifier Model 1800, USA). These signals were then sampled at a rate of 25 kHz (CED Power1401, Cambridge Electronic Design Limited, UK). The process of spike sorting was conducted offline using the Spike2 software (Cambridge Electronic Design Limited, UK).

A photocell (6.5 cm × 6.5 cm, Shenzhen Kobry Technology, China) was attached to the screen. It has the capability to directly capture the temporal information of visual stimuli displayed on the screen at a sampling rate of 1000 Hz by the Spike2 software. The signal was simultaneously recorded with both behavioral and neuronal responses, allowing for precise data analysis.

Saccade video recordings

Saccadic eye movements were assessed in five avian species: pigeon, budgerigar, chukar, chicken, and duck. Birds were observed while awake and head-fixed[35–37] under standard room-light conditions. Additionally, a separate video was recorded from a pigeon resting quietly with its head free to move. A high-speed camera (120 Hz, HONOR Magic6 Pro, China) equipped with an adjustable macro lens (focal length: 30–70 mm, MECORIGHT, China) was used to record their saccadic eye movements.

Retinal tissue preparation and imaging

A pigeon and a chukar were randomly selected for postmortem retinal imaging. Animals were euthanized by the injection of sodium pentobarbital (200 mg/kg) into the pectoral muscles. After euthanasia, the

eyes were enucleated using ophthalmic scissors. Then, a sagittal incision was made along the equator of each eyeball using a sterile scalpel blade to expose the retinal tissue. Images were acquired using the same HONOR Magic6 Pro camera under controlled illumination to minimize glare.

Quantification of saccadic eye movements

A typical saccadic eye movement in birds consists of several oscillations occurring at frequencies of approximately 18–44 Hz. Saccades were identified using a customized detection algorithm implemented in MATLAB. Raw EOG signals were band-pass filtered (5–60 Hz) to remove noise and drift, and peaks and troughs exceeding three times the baseline standard error were detected using MATLAB's *findpeaks* function. Consecutive oscillatory cycles were merged to determine the onset and offset of each saccade. The algorithm was described previously[21] and is publicly available at: https://cdn.elifesciences.org/articles/78729/elife-78729-code1-v1.zip. All detections were subsequently manually verified to ensure accuracy.

To characterize the temporal organization of avian saccadic eye movements, three frequency-related metrics were defined (Fig. 1). Saccade frequency was calculated as the number of detected saccades within each analysis window, representing the rate of occurrence of oscillatory bursts. Oscillation frequency was defined as the total number of oscillatory cycles across all saccadic bursts within the analysis window, representing the overall temporal density of oscillatory activity. Intrasaccadic frequency was defined as the inverse of the duration of each oscillatory cycle, reflecting the temporal frequency of oscillations within individual saccade bursts. Data points lying more than two standard deviations from the mean were considered outliers and excluded.

To quantify the joint influence of saccade and oscillation frequencies, which exhibited partially shared variability, we performed a principal component analysis for each neuron. The first principal component (PC1), capturing the maximal shared variance, was used as a single index of overall saccadic activity. We then computed Pearson correlations between this PC1 and neuronal visual responses across preceding time windows, incrementally ranging from 1 s to 8 min (Fig. 2g, h). To assess the statistical significance of these correlations, we implemented two permutation-based validation procedures following established methods (Supplementary Fig. 8)[66]. First, a within-session ("pseudosession") test was conducted by generating a surrogate time series of trial onsets for each neuron through random shuffling of the original inter-trial intervals. All correlations were recalculated using these surrogate event times ($n = 100$ shuffles) to derive a null distribution. Second, a between-session ("session permutation") test was performed by randomly pairing the complete visual response time series from one neuron with the complete PC1 time series from another neuron ($n = 1000$ permutations). The 95% confidence intervals of these null distributions served as thresholds for statistical significance. We further systematically examined the temporal relationship between saccadic metrics and neuronal responses by combining sliding-window analyses with time-lag assessments (Supplementary Fig. 9).

Glucose levels

The CGM system continuously monitored animals' glucose concentrations. To align with the data of saccade and oscillation, glucose levels were interpolated using a linear method between two consecutive sampled data points. In the light/dark experiments, glucose levels were averaged across three or more repetitions per animal together with corresponding saccadic measures. In the video experiments, only the first transition from the gray screen to the social video was analyzed, when the animals were naïve to such stimuli. To ensure consistency, the values were normalized to the mean glucose level observed during the 30-min baseline period preceding the video, transition of the screen, or the administration of muscimol.

Correlation between saccades and intraocular glucose levels

To investigate the temporal relationship between eye movements and intraocular glucose dynamics, saccade frequency and oscillation frequency were computed within 1-min time windows with a step of 0.1 min and normalized to baseline. To match this sampling rate, intraocular glucose concentrations were linearly interpolated for further analyses. Data were averaged across trials for each animal and subsequently pooled across individuals.

A lag correlation analysis was then performed to assess temporal coupling between eye movements and intraocular glucose levels. Because glucose fluctuations evolve on a slower timescale than saccadic eye movements, we applied a modified cross–correlation approach to minimize spurious correlations arising from slow drifts and strong autocorrelation. Both signals were z-score normalized to standardize amplitude, followed by linear detrending to suppress slow variations and reduce artificial correlations at negative lags. The cross-correlation function was computed with a temporal resolution matched to the sampling interval used for cross-animal averaging. To determine statistical significance, a null distribution was generated by randomly shuffling one signal relative to the other 1000 times. Observed correlation values at each lag were compared with the 95% confidence interval of the null distribution, and only values exceeding this range were considered significant. Positive lags indicate that glucose changes followed saccadic activity, whereas negative lags indicate the reverse.

To further validate the lag interval between intraocular glucose concentrations and saccades, we applied a standard-deviation (SD)-based threshold method (Supplementary Fig. 4). For each signal, a 30-min period preceding the state change (visual stimuli switch or muscimol injection) was defined as the baseline. The mean and standard deviation of the baseline period were calculated for each pigeon, and the response threshold was set at 2.5 times the SD beyond the baseline mean (Threshold = mean ± 2.5 × SD). Starting from the onset of the state change, we examined the subsequent time series and identified the first time point at which the signal exceeded or fell below this threshold. This time point was defined as the response latency for each individual, and the mean latency was then averaged across animals. Because visual scenes during the social-mating video sessions were highly variable and fragmented, eliciting enhanced yet dynamically fluctuating eye movements, the SD-based latency analysis was applied only to the light/dark screen and pharmacological conditions. Under these conditions, visual stimuli were consistent and uniform, producing stable and well-defined eye-movement patterns that allowed reliable latency estimation.

Neuronal visual responses

We successfully identified firing activity in 127 neurons from three retinorecipient structures in the visual pathways of birds. Neuronal firing rates were computed using established methods[67] and averaged in 50-ms bins. In order to eliminate the influence of perisaccadic modulations on visual response analyses, we first quantified the temporal extent of these modulations by aligning neuronal firing rates to the onset and offset of saccades for each neuron. The duration of perisaccadic modulation was determined using a standard-deviation-based criterion, identifying the time point where the firing rate consistently returned to the stable baseline within a specified statistical tolerance. All visual response data within these modulation time frames were excluded, thereby restricting analyses to stable fixation periods and isolating them from perisaccadic modulations.

In this study, a 300 ms grating motion served as a probe to assess neuronal visual responses. We calculated the average spontaneous firing rates during saccade intervals without probes, aligned to the

onset of the prior saccade. For each probe, the mean spontaneous firing rate within a 300-ms window, aligned to the probe timing relative to the prior saccade, was used as the baseline. Visual responses to the grating motion were then defined by subtracting this baseline. To assess the relationship between visual responses and the prior saccade, we calculated the distribution of time intervals between the two events, excluded the 5% extreme values, and divided the remaining intervals equally into three stages. We then compared neuronal visual responses across these stages (Fig. 3), as well as before and after microinjections (Fig. 4). In the muscimol administration experiment, saccades were suppressed, and the average firing rates within a 100 ms time interval preceding the grating motion were calculated as a baseline for comparing neuronal visual responses before and after muscimol administration (Fig. 5). To assess post-injection latency, neuronal activity was aligned to injection onset and analyzed in 0.5-min windows. Neuronal visual responses were z-score normalized to the pre-injection baseline (excluding outliers exceeding 3 standardized MAD), and latency was defined as the first window showing a significant deviation from baseline.

Modeling of intraocular glucose dynamics

To approximate intraocular glucose perfusion in pigeons, we developed a simplified one-dimensional diffusion model incorporating both metabolic consumption and saccade-driven mechanical oscillations. This framework was inspired by Pettigrew's classic study in the tawny frogmouth, which showed that fluorescein dye can be rapidly transported ~2–3 mm from the pecten within 2 s of a single saccade[29], whereas passive diffusion during fixation is negligible (<0.5 mm even after 120 s). These findings suggest that saccade substantially enhances nutrient delivery from the pecten. Given the complex three-dimensional nature of ocular fluid flow and metabolism, we reduced the system to a one-dimensional diffusion domain extending from the pecten to the retinal periphery. The glucose concentration $c(x, t)$ over space x and time t follows *Fick's second law* with an additional consumption term R and an oscillatory flow component $v(x, t)$:

$$\frac{\partial c}{\partial t} = D\frac{\partial^2 c}{\partial x^2} - R + v(x,t)\frac{\partial c}{\partial x} \tag{1}$$

where D is the diffusion coefficient, and $v(x,t)$ models periodic fluid motion driven by saccadic oscillations. Under the small-amplitude approximation and Taylor dispersion theory, the concentration at positions a and b can be expressed as:

$$\begin{aligned} c(x,t) = {} & c_1 + \left(\tfrac{c_2-c_1}{L}\right)x + \tfrac{R}{2D_{eff}}\left(x^2 - Lx\right) \\ & + \tfrac{A\omega e^{-\alpha x}}{Dk^2}\left[\tfrac{c_2-c_1}{L} + \tfrac{R}{D_{eff}}\left(x - \tfrac{L}{2}\right)\right]\cos\left(\omega t - kx + \phi_0\right) \\ & + \tfrac{A\omega^2 e^{-\alpha x}}{Dk^3}\left[\tfrac{c_2-c_1}{L} + \tfrac{R}{D_{eff}}\left(x - \tfrac{L}{2}\right)\right]\sin(\omega t - kx + \phi_0) \end{aligned} \tag{2}$$

The effective diffusion coefficient incorporating the oscillatory component is given by:

$$D_{eff} = D + \frac{(A\omega)^2}{2Dk^2}\left(\frac{1}{1} + (\omega/(Dk^2))^2\right) \tag{3}$$

Parameter values were based on published physiological data. The pigeon eye was modeled as a sphere of radius $L = 7$ mm (ocular diameter of ~13–14 mm)[68]. Two retinal locations were examined: a proximal site 1 mm from the pecten (position a) and a distal site 4 mm away (position b). Blood glucose levels in birds typically range between 13–15 mmol/L; we therefore set $c_1 = 15$ mmol/L at the pecten and $c_2 = 13$ mmol/L at the retinal edge[69]. The glucose consumption rate R was estimated from pigeon brain metabolism (27.29 ± 1.57 µmol glucose per 100 g per min $\approx 4.55 \times 10^{-4}$ mmol L^{-1} s^{-1})[2]. The diffusion coefficient of glucose in water at 39 °C is 0.92×10^{-9} m^2/s; corrected to 40 °C using the Stokes–Einstein relation and adjusted for vitreous medium (~twofold reduction), this yields $D = 4.68 \times 10^{-4}$ mm^2/s[70,71]. The oscillatory term was parameterized by the saccade frequency distribution. Using the 95% confidence bound of inter-saccade intervals (7.57 s in our data), the mechanical oscillation frequency was set to $f = 0.13$ Hz. Based on this frequency, the wave number ($k = 12.81$ rad/mm), angular frequency ($\omega = 0.83$ rad/s), and phase ($\varphi_0 = 0.97\pi$ rad) were used to determine the relative timing of proximal and distal glucose oscillations. The oscillation amplitude A was taken as one-tenth of the system length (0.7 mm), and the decay coefficient as $\alpha = 1 \times 10^{-3}$ mm^{-1}.

Numerical simulations revealed temporal glucose concentration profiles at both retinal sites a and b. The saccade introduced phase-dependent fluctuations and concentrations, producing asynchronous glucose peaks between proximal and distal locations after a saccade (Fig. 3). These dynamics qualitatively match experimentally observed differences in neuronal responses within the optic tectum, supporting the hypothesis that saccades modulate retinal metabolism through pecten-driven perfusion. While the present model simplifies the three-dimensional fluid mechanics of the avian vitreous, it could provide the key temporal and spatial trends of glucose distribution within the eye. Estimated glucose signals were normalized by dividing each waveform by its peak-to-peak amplitude at the corresponding recording site.

Statistical analysis

A two-sided Wilcoxon signed-rank test was utilized to assess behavioral and neuronal visual responses for paired data, whereas the Wilcoxon rank-sum test was applied to independent observations. To examine the effect of visual conditions on eye movement metrics (Fig. 1), we performed one-way Analysis of Variance (ANOVA) followed by Tukey's HSD post-hoc tests for pairwise comparisons. To further account for the non-independence of repeated measurements within animals, we fitted a linear mixed-effects model for each frequency metric, with the visual condition as a fixed effect and pigeon identity as a random intercept (*Frequency ~ Condition + (1 | Pigeon ID)*). Post-hoc comparisons for the LMM analysis were conducted using Wald tests. Visual responses across the three stages following saccades were compared using a one-way analysis of variance (one-way ANOVA). Partial correlation (Supplementary Fig. 11) was used to assess the independent contribution of correlated variables (saccade duration, oscillatory cycle count, and time since last saccade) to visual responses. The Holm-Bonferroni correction was applied to control for multiple comparisons. Statistical analysis was conducted with a significance level of 0.05.

Figure preparation

The schematic illustrations and drawings presented in Figs. 1a, b, p, 2a, b, 3j, 4a, b, 5a and Supplementary Fig. 5a were initially created using Procreate (version 5.4.7, Savage Interactive Pty Ltd) and finalized using Adobe Illustrator 2022 (Adobe Inc.).

Reporting summary

Further information on research design is available in the Nature Portfolio Reporting Summary linked to this article.

Data availability

Source data are provided with this paper. The data that support the findings of this study are available in the Source Data file. Source data are provided with this paper.

Code availability

The customized algorithm for saccade detection was reported in our previous study[21] and is publicly available at: https://cdn.elifesciences.

org/articles/78729/elife-78729-code1-v1.zip. A detailed description of the customized MATLAB algorithm is provided in the Methods section.

References

1. Nagy, K. A., Girard, I. A. & Brown, T. K. Energetics of free-ranging mammals, reptiles, and birds. *Annu. Rev. Nutr.* **19**, 247–277 (1999).
2. Von Eugen, K. et al. Avian neurons consume three times less glucose than mammalian neurons. *Curr. Biol.* **32**, 4306–4313.e4304 (2022).
3. Baden, T., Euler, T. & Berens, P. Understanding the retinal basis of vision across species. *Nat. Rev. Neurosci.* **21**, 5–20 (2020).
4. Meyer, D. B. In *The Visual System in Vertebrates* (eds Crescitelli, F. et al.) 549–611 (Springer, 1977).
5. Caves, E. M., Brandley, N. C. & Johnsen, S. Visual acuity and the evolution of signals. *Trends Ecol. Evol.* **33**, 358–372 (2018).
6. Martin, G. R. Avian vision. *Curr. Biol.* **32**, R1079–r1085 (2022).
7. Evans, H. E. in *Handbook of Bird Biology* (eds Lovette, I.J. & Fitzpatrick, J.W.) 169–213 (Wiley, 2016).
8. Shimizu, T. & Watanabe, S. in *How Animals See the World: Comparative Behavior, Biology, and Evolution of Vision* (eds Lazareva, O. F., Shimizu, T. & Wasserman, E.A.) 26–43 (Oxford University Press, 2012).
9. Reiner, A., Fitzgerald, M. E. C., Del Mar, N. & Li, C. Neural control of choroidal blood flow. *Prog. Retin. Eye Res.* **64**, 96–130 (2018).
10. McKibbin, M. et al. Spectral domain optical coherence tomography imaging of the posterior segment of the eye in the retinal dysplasia and degeneration chicken, an animal model of inherited retinal degeneration. *Vet. Ophthalmol.* **17**, 113–119 (2014).
11. Hughes, J., Jerrome, D. & Krebs, H. Ultrastructure of the avian retina an anatomical study of the retina of the domestic pigeon (Columba liva) with particular reference to the distribution of mitochondria. *Exp. Eye Res.* **14**, 189–195 (1972).
12. Ruggeri, M. et al. Retinal structure of birds of prey revealed by ultra-high resolution spectral-domain optical coherence tomography. *Investig. Ophthalmol. Vis. Sci.* **51**, 5789–5795 (2010).
13. Dubielzig, R. R., Ketring, K., McLellan, G. J. & Albert, D. M. in *Veterinary Ocular Pathology* (eds Dubielzig, R. R., Ketring, k., McLellan, G. J. & Albert, D. M.) 349–397 (W.B., 2010).
14. Williams, D. Eagle eyed or bird brained? *Eye* **37**, 2426–2430 (2023).
15. Catita, J. et al. Imaging of cellular aging in human retinal blood vessels. *Exp. Eye Res.* **135**, 14–25 (2015).
16. Adams, D. L. & Horton, J. C. The representation of retinal blood vessels in primate striate cortex. *J. Neurosci.* **23**, 5984–5997 (2003).
17. Provis, J. M. Development of the primate retinal vasculature. *Prog. Retin. Eye Res.* **20**, 799–821 (2001).
18. Nye, P. W. The monocular eye movements of the pigeon. *Vis. Res.* **9**, 133–144 (1969).
19. Marin, G., Letelier, J. C. & Wallman, J. Saccade-related responses of centrifugal neurons projecting to the chicken retina. *Exp. Brain Res.* **82**, 263–270 (1990).
20. Yang, Y., Yang, Y. & Wang, S.-R. Neuronal circuitry and discharge patterns controlling eye movements in the pigeon. *J. Neurosci.* **28**, 10772–10780 (2008).
21. Xiao, T. et al. Sensory input-dependent gain modulation of the optokinetic nystagmus by mid-infrared stimulation in pigeons. *eLife* **12**, https://doi.org/10.7554/eLife.78729 (2023).
22. Yang, Y., Cao, P., Yang, Y. & Wang, S.-R. Corollary discharge circuits for saccadic modulation of the pigeon visual system. *Nat. Neurosci.* **11**, 595–602 (2008).
23. Tyrrell, L. P., Butler, S. R. & Fernández-Juricic, E. Oculomotor strategy of an avian ground forager: tilted and weakly yoked eye saccades. *J. Exp. Biol.* **218**, 2651–2657 (2015).
24. Voss, J. & Bischof, H. J. Eye movements of laterally eyed birds are not independent. *J. Exp. Biol.* **212**, 1568–1575 (2009).
25. Pratt, D. W. Saccadic eye movements are coordinated with head movements in walking chickens. *J. Exp. Biol.* **97**, 217–223 (1982).
26. Bloch, S., Rivaud, S. & Martinoya, C. Comparing frontal and lateral viewing in the pigeon. III. Different patterns of eye movements for binocular and monocular fixation. *Behav. Brain Res.* **13**, 173–182 (1984).
27. Lemeignan, M., Sansonetti, A. & Gioanni, H. Spontaneous saccades under different visual conditions in the pigeon. *Neuroreport* **3**, 17–20 (1992).
28. Yorzinski, J. L. & Platt, M. L. Selective attention in peacocks during predator detection. *Anim. Cogn.* **17**, 767–777 (2014).
29. Pettigrew, J. D., Wallman, J. & Wildsoet, C. F. Saccadic oscillations facilitate ocular perfusion from the avian pecten. *Nature* **343**, 362–363 (1990).
30. Wood, C. A. *The Fundus Oculi of Birds: Especially as Viewed by the Ophthalmoscope; A Study in the Comparative Anatomy and Physiology*. (Lakeside Press, 1917).
31. Ringvold, A. The pecten oculi: an enigma in comparative ophthalmology. *Eur. J. Appl. Sci.* **11**, 81–88 (2023).
32. Brach, V. The functional significance of the avian pecten: a review. *Condor* **79**, 321–327 (1977).
33. Christensen, N. K., Beedholm, K. & Damsgaard, C. Short communication: maintained visual performance in birds under high altitude hypoxia. *Comp. Biochem. Physiol. Part A Mol. Integr. Physiol.* **296**, 111691 (2024).
34. Osborne, N. N. et al. Retinal ischemia: mechanisms of damage and potential therapeutic strategies. *Prog. Retin. Eye Res.* **23**, 91–147 (2004).
35. Neuenschwander, S., Engel, A. K., König, P., Singer, W. & Varela, F. J. Synchronization of neuronal responses in the optic tectum of awake pigeons. *Vis. Neurosci.* **13**, 575–584 (1996).
36. Mahajan, N. R. & Mysore, S. P. Donut-like organization of inhibition underlies categorical neural responses in the midbrain. *Nat. Commun.* **13**, 1680 (2022).
37. Xiao, G. et al. Mesoscale neuronal granular trial variability in vivo illustrated by nonlinear recurrent network in silico. *Nat. Commun.* **15**, 9894 (2024).
38. Clark, W. J. & Colombo, M. The functional architecture, receptive field characteristics, and representation of objects in the visual network of the pigeon brain. *Prog. Neurobiol.* **195**, 101781 (2020).
39. Cao, P., Gu, Y. & Wang, S. R. Visual neurons in the pigeon brain encode the acceleration of stimulus motion. *J. Neurosci.* **24**, 7690–7698 (2004).
40. Wylie, D. R., Gutierrez-Ibanez, C., Pakan, J. M. & Iwaniuk, A. N. The optic tectum of birds: mapping our way to understanding visual processing. *Can. J. Exp. Psychol.* **63**, 328–338 (2009).
41. Remy, M. & Güntürkün, O. Retinal afferents to the tectum opticum and the nucleus opticus principalis thalami in the pigeon. *J. Comp. Neurol.* **305**, 57–70 (1991).
42. Güntürkün, O. Morphological asymmetries of the tectum opticum in the pigeon. *Exp. Brain Res.* **116**, 561–566 (1997).
43. Jarvis, E. D. et al. Avian brains and a new understanding of vertebrate brain evolution. *Nat. Rev. Neurosci.* **6**, 151–159 (2005).
44. Pusch, R., Clark, W., Rose, J. & Güntürkün, O. Visual categories and concepts in the avian brain. *Anim. Cogn.* **26**, 153–173 (2023).
45. Stacho, M. et al. A cortex-like canonical circuit in the avian forebrain. *Science* **369**, https://doi.org/10.1126/science.abc5534 (2020).
46. Basso, M. A., Bickford, M. E. & Cang, J. Unraveling circuits of visual perception and cognition through the superior colliculus. *Neuron* **109**, 918–937 (2021).
47. McGill, J. I., Powell, T. P. & Cowan, W. M. The retinal representation upon the optic tectum and isthmo-optic nucleus in the pigeon. *J. Anat.* **100**, 5–33 (1966).

48. Hamdi, F. A. & Whitteridge, D. The representation of the retina on the optic tectum of the pigeon. *Q J. Exp. Physiol. Cogn. Med. Sci.* **39**, 111–119 (1954).
49. Ban, Y. & Rizzolo, L. J. Regulation of glucose transporters during development of the retinal pigment epithelium. *Brain Res. Dev. Brain Res.* **121**, 89–95 (2000).
50. Gerhardt, H., Liebner, S. & Wolburg, H. The pecten oculi of the chicken as a new in vivo model of the blood-brain barrier. *Cell Tissue Res.* **285**, 91–100 (1996).
51. Zhang, R., Kang, R. & Tang, D. Reductive cell death: the other side of the coin. *Cancer Gene Ther.* **30**, 929–931 (2023).
52. Ma, Y. et al. Ovarian cancer relies on glucose transporter 1 to fuel glycolysis and growth: anti-tumor activity of BAY-876. *Cancers* **11**, https://doi.org/10.3390/cancers11010033 (2018).
53. Siebeneicher, H. et al. Identification and optimization of the first highly selective GLUT1 inhibitor BAY-876. *ChemMedChem* **11**, 2261–2271 (2016).
54. Country, M. W. Retinal metabolism: a comparative look at energetics in the retina. *Brain Res.* **1672**, 50–57 (2017).
55. Boyle, J. Lehninger principles of biochemistry (4th ed.): Nelson, D., and Cox, M. *Biochem. Mol. Biol. Educ.* **33**, 74–75 (2005).
56. Rudney, H. The utilization of L-glucose by mammalian tissues and bacteria. *Science* **92**, 112–113 (1940).
57. Bruton, J., Horner, W. H. & Russ, G. A. Biosynthesis of streptomycin. IV. Further studies on the biosynthesis of streptidine and N-methyl-L-glucosamine. *J. Biol. Chem.* **242**, 813–818 (1967).
58. Jarvis, E. D. et al. Whole-genome analyses resolve early branches in the tree of life of modern birds. *Science* **346**, 1320–1331 (2014).
59. Yang, Y., Wang, Q., Wang, S. R., Wang, Y. & Xiao, Q. Representation of time interval entrained by periodic stimuli in the visual thalamus of pigeons. *eLife* **6**, https://doi.org/10.7554/eLife.27995 (2017).
60. Karten, H. J. & Hodos, W. *A Stereotaxic Atlas of the Brain of the Pigeon:(Columba Livia)*. Vol. 696 (Johns Hopkins Press, 1967).
61. Azizpour, A. & Hassani, Y. Clinical evaluation of general anaesthesia in pigeons using a combination of ketamine and diazepam. *J. S Afr. Vet. Assoc.* **83**, 12 (2012).
62. Britto, L. R., Gasparotto, O. C. & Hamassaki, D. E. Visual telencephalon modulates directional selectivity of accessory optic neurons in pigeons. *Vis. Neurosci.* **4**, 3–10 (1990).
63. Fu, Y. X., Gao, H. F., Guo, M. W. & Wang, S. R. Receptive field properties of visual neurons in the avian nucleus lentiformis mesencephali. *Exp. Brain Res.* **118**, 279–285 (1998).
64. Fuchs, A. F. & Luschei, E. S. Unit activity in the brainstem related to eye movement. Possible inputs to the motor nuclei. *Bibl. ophthalmol. Suppl. ad ophthalmol.* **82**, 17–27 (1972).
65. Wohlschläger, A., Jäger, R. & Delius, J. D. Head and eye movements in unrestrained pigeons (Columba livia). *J. Comp. Psychol.* **107**, 313 (1993).
66. Harris, K. D. Nonsense correlations in neuroscience. Preprint at https://doi.org/10.1101/2020.11.29.402719 (2021).
67. Lisberger, S. G. & Pavelko, T. A. Vestibular signals carried by pathways subserving plasticity of the vestibulo-ocular reflex in monkeys. *J. Neurosci.* **6**, 346–354 (1986).
68. Donovan, W. J. Structure and function of the pigeon visual system. *Physiol. Psychol.* **6**, 403–437 (1978).
69. Braun, E. J. & Sweazea, K. L. Glucose regulation in birds. *Comp. Biochem. Physiol. Part B Biochem. Mol. Biol.* **151**, 1–9 (2008).
70. Koirala, R. P., Dawanse, S. & Pantha, N. Diffusion of glucose in water: a molecular dynamics study. *J. Mol. Liq.* **345**, 117826 (2022).
71. Del Amo, E. M. et al. Pharmacokinetic aspects of retinal drug delivery. *Prog.Retin. Eye Res.* **57**, 134–185 (2017).

Acknowledgements

We thank Shu-Rong Wang (Institute of Biophysics), Sheng He (Institute of Biophysics), Guangwei Si (Institute of Biophysics), and members of our laboratory for their advising and commenting on the manuscript, Zhenyu Gao (Erasmus MC) for helpful discussions. Yanhui Fu (Institute of Biophysics) and Haiyan Liu (Institute of Biophysics) for their invaluable technical assistance. This work was supported by the Brain Science and Brain-like Intelligence Technology, National Science and Technology Major Project (2021ZD0203800 to X.X., T.X., and T.Z.; 2022ZD0204800 to Y.Y.), the Chinese Academy of Sciences Key Program of Frontier Sciences (QYZDB-SSW-SMC019 to Y.Y.), the National Natural Science Foundation of China (31722025 and 32070987 to Y.Y.), and the Strategic Priority Research Program of the Chinese Academy of Sciences (XDB37030303 to Y.Y.).

Author contributions

Conceptualization: Y.Y. Methodology: Y.Y., X.X., T.X., and Y.B.C. Investigation: X.X., T.X., Y.B.C., L.J.S., C.W., and Q.W. Visualization: X.X., T.X., Y.B.C., and Y.Y. Funding acquisition: Y.Y. Project administration: Y.Y. Supervision: Y.Y. Writing—original draft: Y.Y., X.X. Writing—review and editing: Y.Y., X.X., T.X., Y.B.C., and T.Z.

Competing interests

The authors declare no competing interests.

Additional information

Supplementary information The online version contains supplementary material available at https://doi.org/10.1038/s41467-026-70672-0.

Correspondence and requests for materials should be addressed to Yan Yang.

Peer review information *Nature Communications* thanks Onur Güntürkün and the other anonymous reviewer(s) for their contribution to the peer review of this work. A peer review file is available.